Annals of Glaciology 35 2002

Ice-flow properties at Dome Summit South, Law Dome, East Antarctica

WEILI WANG,[1] ROLAND C. WARNER,[2,3] WILLIAM F. BUDD[3]
[1]*Raytheon ITSS, Oceans and Ice Branch, NASA Goddard Space Flight Center, Code 971, Greenbelt, MD 20771, U.S.A.*
E-mail: weili@icesat2.gsfc.nasa.gov
[2]*Australian Antarctic Division and* [3]*Antarctic CRC, Box 252-80, Hobart, Tasmania 7001, Australia*

ABSTRACT. Ice-flow properties within a polar ice sheet are examined using the comprehensive data gathered from ice-core drilling by Australian National Antarctic Research Expeditions (ANARE) at Dome Summit South (DSS), on Law Dome, East Antarctica. Using the shear strain rates derived from borehole inclination measurements we demonstrate the need to modify the ice-flow relations to treat enhanced shear deformation deep within the ice sheet. We show that the relation between enhanced flow and the measured crystallographic properties is generally in accord with expectations, at least in the upper parts of the ice sheet, but it becomes clear that nearer to the bedrock the situation is more complicated. We also compare the observed shear strain-rate profile with results from a model that describes flow enhancement as a function of the applied stresses.

1. INTRODUCTION

Ice-core drilling on Law Dome, East Antarctica, by Australian National Antarctic Research Expeditions (ANARE) of a 1200 m borehole at Dome Summit South (DSS), at 66°46′11″ S, 112°48′25″ E, 4.6 km south-southwest of the summit of the dome during the 1987–93 summer seasons, has provided an excellent opportunity to investigate ice-flow properties within an ice sheet. DSS is not only the deepest borehole drilled in Law Dome but also has the most complete set of observations. Observations of shear strain rates from changes in borehole inclination and borehole temperature measurements (Morgan and others, 1997, 1998), and physical (Li, 1995; Li and others, 1998) and chemical (Curran and others, 1998; Edwards and others, 1998; Rosman and others, 1998) analyses of the ice core are all available. Here we consider the information about ice-flow properties that these measurements reveal.

The shear strain rate increases with depth to a maximum located approximately 200 m above the bedrock and then decreases considerably. We demonstrate the necessity of modifying the treatment of the shear deformation of ice, beyond the conventional influences of increasing shear stress and temperature with depth in the ice sheet. Using a parameterization of flow relations, related to previous Antarctic modelling studies and laboratory ice-deformation experiments, an "enhancement factor" can be calculated as the ratio of the observed strain rate to the strain rate that would be produced on isotropic ice under the same stresses. We show that the relation between this enhancement factor and the measured crystallographic properties is generally in accord with expectations, at least in the upper parts of the ice sheet, but it becomes clear that the shear stress cannot be treated as a linear function of depth throughout the ice sheet. The presence of a maximum shear strain rate at some distance above the bedrock is also observed in other boreholes drilled by ANARE along a transect from the summit of Law Dome to the coast (Russell-Head and Budd, 1979; Etheridge, 1989). These strain-rate profiles were modelled in a study of anisotropic ice flow by Wang and Warner (1999). With the comprehensive collection of data available at DSS, linking the degree of shear flow enhancement to crystallographic quantities, such as ice crystal-fabric verticality, or to other variables considered in previous modelling studies, gives some indications of the way the shear stress may actually vary in the lower layers of the ice sheet, and points once again to the importance of a better understanding of flow in these regions.

2. FLOW PROPERTIES

Several results from the borehole measurements and the ice-core studies that are of interest here are shown in Figure 1. There appears to be a systematic increase with depth of both the shear strain rate (Fig. 1b) and the verticality of the fabric of the ice crystal structure, represented in Figure 1e by the parameter $\phi(1/4)$ which indicates the half-apex angle of the cone about the vertical containing the *c*-axis directions of 25% of the ice crystals measured in an ice-core thin section, until the depth of the maximum shear rate at about 1000 m. Below that depth the decrease in shear strain rate is associated with a tendency for increased crystal size (Fig. 1c) and a decrease in ice fabric strength favorable for horizontal shear, i.e. a trend away from small values of $\phi(1/4)$, except around 1113 m depth where a narrow spike of very high shear is associated with ice from the Last Glacial Maximum (LGM). This thin layer of ice has relatively high levels of dust (Fig. 1d) and chemical impurities (Edwards and others, 1998) and small crystals with strong, vertically oriented, single-maximum *c*-axis fabrics. From the intercomparison study of ice-deformation experiments on ice from different ice cores by Wang (1994) it appears that the strongly favourable crystal fabric for shear is the main reason for the higher shear rate of this

https://doi.org/10.3189/172756402781816924 Published online by Cambridge University Press

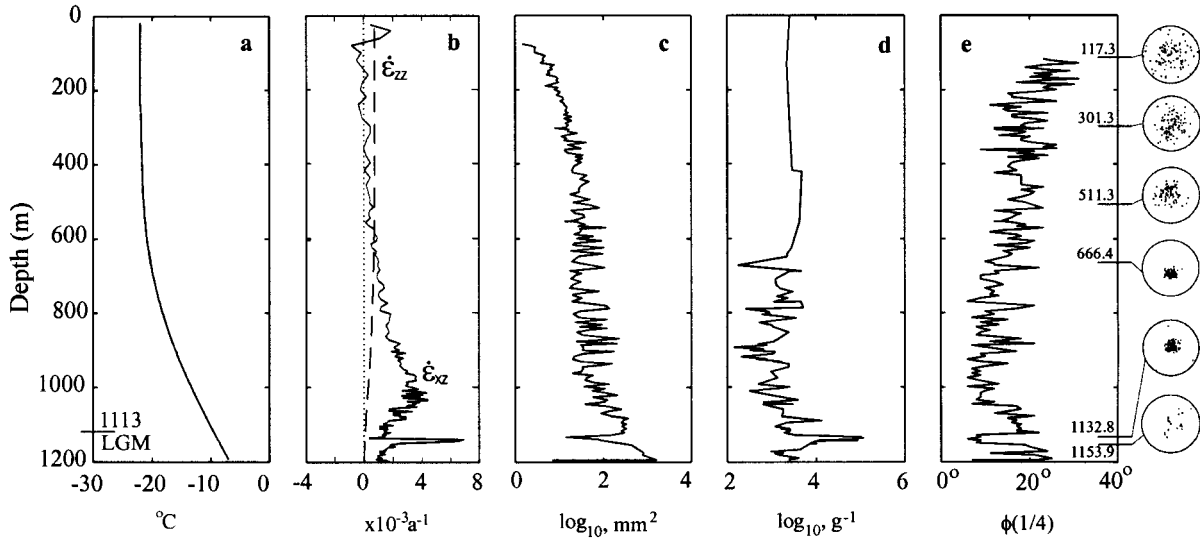

Fig. 1. The measured profiles of: (a) borehole temperature (T) (from Morgan and others, 1998); (b) horizontal shear strain rate ($\dot{\varepsilon}_{xz}$) (solid line) derived from the borehole inclination measurements (from Morgan and others, 1998) and derived vertical compressive strain rate ($\dot{\varepsilon}_{zz}$) (dashed line); (c) mean crystal size (from Li and others, 1998); (d) microparticle concentration of particles with diameters > 0.506 μm (from Li and others, 1998); and (e) fabric parameter ϕ(1/4), the half-apex angles of the cones containing 25% of the c axes, and selected fabric diagrams (from Li, 1995).

ice, rather than the impurity content. However, it appears that the preservation of the strong single maximum with small crystals in this layer is due to the retardation of the recrystallization and crystal growth by the high level of impurities as shown by Li and others (1998). The studies at Dye 3 borehole, Greenland, suggest that part of the enhanced flow for Wisconsin ice near the bottom of that borehole may be due to impurities or crystal size (Dahl-Jensen, 1985; Dahl-Jensen and Gundestrup, 1987; Thorsteinsson and others, 1999). The LGM layer at DSS is very thin and does not contribute greatly to the total shear. Therefore we focus here on the general increase in shear rate down to the maximum shear layer (at just below 1000 m) and a reduction in shear strain rate below that depth, which we attribute to the general influence of large-scale bedrock roughness.

Flow law, flow-law parameters and enhancement factor

The isotropic flow law for ice (Glen, 1955, 1958) may be expressed in the relations between strain rates ($\dot{\varepsilon}_{ij}$) and stresses (τ_{ij}) for components of shear and compression as

$$\dot{\varepsilon}_{xz} = B\tau_{\mathrm{o}}^{n-1}\tau_{xz} \tag{1}$$

$$\dot{\varepsilon}_{zz} = B\tau_{\mathrm{o}}^{n-1}\tau'_{zz}\,, \tag{2}$$

where the subscripts xz and zz denote horizontal shear and vertical compression, respectively, τ'_{zz} denotes the appropriate component of the deviatoric stress tensor, B is the flow-law parameter; n the flow-law exponent is taken equal to 3 in the present work; and the octahedral shear stress (τ_{o}) is calculated from the deviatoric stresses, and may be expressed as

$$\tau_{\mathrm{o}} = \sqrt{\frac{2}{3}(\tau_{xz}^2 + \tau_{zz}'^2)}\,, \tag{3}$$

for the case of ice flow corresponding to a confined vertical compression stress combined with a horizontal shear stress τ_{xz}. In ice sheets the shear stress τ_{xz} is frequently calculated by assuming a linear increase with the depth all the way to the bed as

$$\tau_{xz} = \rho g \alpha z \tag{4}$$

in terms of the ice density ρ, the acceleration due to gravity g, the mean surface slope α (taken here as 0.007, averaged along the flowline over 5 times the ice thickness at the DSS site) and the ice depth z.

For the present study we generalize Equations (1) and (2) by the introduction of a single, variable enhancement factor E into the parameter B, which is taken here as

$$B = EA_{\mathrm{o}}(T) = EA' \exp(-Q/RT)\,, \tag{5}$$

where the factor E may involve the effects of ice fabric, ice crystal size and impurities on the deformation of the ice. $A_{\mathrm{o}}(T)$ is the temperature-dependent parameter representing the minimum octahedral creep rate per unit octahedral shear stress for ice with an isotropic crystal fabric, expressed in terms of A', a constant, the activation energy Q (40 kJ mol^{-1}; Weertman, 1973), the gas constant R (8.314 J mol^{-1} K^{-1}) and the absolute temperature T. From Equations (1) and (2) it is clear that the single enhancement factor E represents an enhancement of the flow law relating octahedral strain rate to octahedral shear stress, relative to the isotropic case, and it can be compared with a similar quantity extracted from laboratory experiments involving combined shear and compression loads by Li and others (1996). A model treating separate enhancement functions for shear and compression was outlined by Wang and Warner (1999), but as one of the main purposes of the present paper is to extract an estimate of enhancement from analysis of measured shear strain rates, we consider here a single depth-dependent function E. This enhancement factor tends to the corresponding enhancement for the shear component of flow when that component is dominant (see Wang and Warner (1999) for details). Note that the assumption of a common E factor is essential to the simple elimination of the unknown compressive deviatoric stress τ'_{zz} in favour of the shear stress and the strain rates.

https://doi.org/10.3189/172756402781816924 Published online by Cambridge University Press

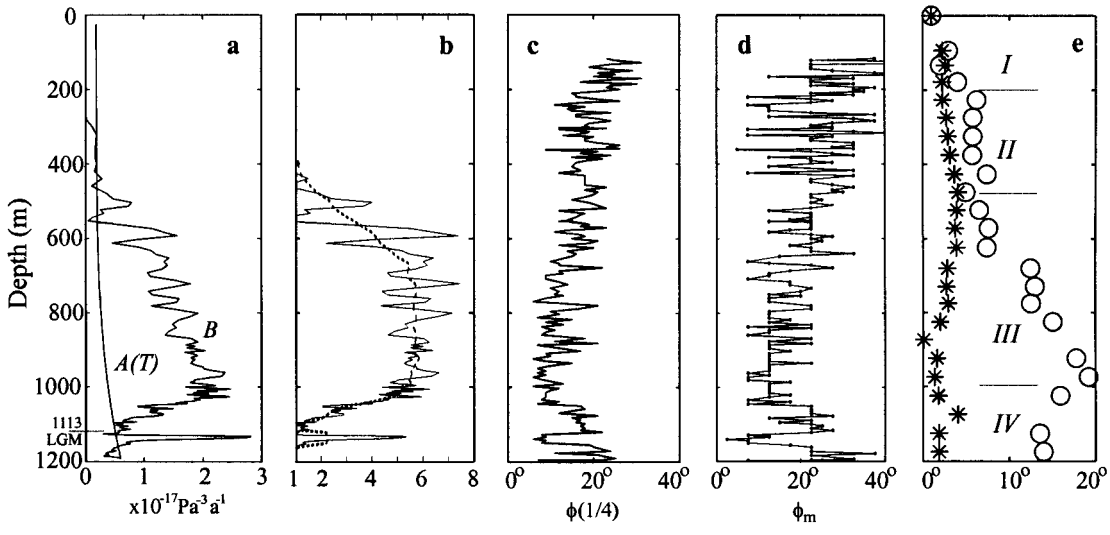

Fig. 2. The profiles of (a) flow-law parameter B, and temperature parameter $A_o(T)$; (b) enhancement factor E^{obs} (solid line), and smoothed fit (dashed line); (c) fabric parameter $\phi(1/4)$; (d) fabric parameter ϕ_m, the modal value from the histogram plot of crystal number vs c-axis co-latitude angle (in 5° bins); (e) normalized ratios from fabric analysis. The ratios R_{20-30} and R_{0-15} are, respectively, the percentage of the co-latitudes of all measured c axes falling within 20–30° and 0–15° of the vertical, normalized by the corresponding values for a randomly distributed fabric. Four crystallographic zones (I–IV) are indicated, with boundaries at 200, 450 and 1000 m.

From Equations (1–3), the flow relation can be rewritten as

$$\dot{\varepsilon}_{xz}^3 - \frac{2}{3} B \tau_{xz}^3 (\dot{\varepsilon}_{xz}^2 + \dot{\varepsilon}_{zz}^2) = 0 \,. \qquad (6)$$

The flow-law parameter B can be obtained from the above equation once the vertical strain rate $\dot{\varepsilon}_{zz}$ is known, since the shear strain rate $\dot{\varepsilon}_{xz}$ is available from the borehole inclination measurements (Fig. 1b) and the shear stress can be calculated from Equation (4).

Here we use an approach to calculate vertical strain rate under steady-state conditions, based on the assumption that ice is incompressible and that the depth profile of horizontal velocity varies only slowly along the flowline:

$$\dot{\varepsilon}_{zz} = -\dot{\varepsilon}_{xx} = -\frac{\partial U}{\partial x} = \frac{\partial U}{\partial z}\alpha z + \frac{U}{D}\alpha - \frac{a}{D}\psi \,, \qquad (7)$$

where the coordinate x is taken along the flow direction, $U(z)$ is the depth-dependent horizontal velocity integrated from the measured shear strain rate (Fig. 1b), a is the surface accumulation rate (0.678 m a^{-1} at DSS, taking a 50 year average), D is the total ice thickness (1177 m, averaged over 5 times the ice thickness, along the flowline at the DSS site), and ψ is a function of depth which gives the shape of the horizontal velocity as a function of the depth z:

$$\psi(z) = \frac{U(z)}{\dfrac{1}{D}\displaystyle\int_{\text{bed}}^{\text{surface}} U(z)|\mathrm{d}z|} \,. \qquad (8)$$

To demonstrate the extent of the enhanced flow, the enhancement factor E^{obs} is then calculated from Equation (5) using B obtained from Equation (6) and A' chosen to make the mean value of the enhancement factor (E^{obs}) equal to 1 for the top 400 m depth of the borehole.

Relationship of enhancement factor to fabric

The flow-law parameter B, the temperature-dependent parameter $A_o(T)$ and the enhancement factor E^{obs} are shown in Figure 2a and b for comparison with various measures of the ice crystal fabric in Figure 2c–e. The fabric measurements (Li, 1995) involve 185 fabrics, typically at 5–10 m spacing, with over 100 measured c axes per fabric.

Figure 2b shows that significant enhancement starts at around 500 m depth, where the shear and compression strain rates become comparable. It then increases rapidly (although the variability in the measurements produces scatter in the estimates of enhancement), and from 700 to 1000 m the values cluster around 6, with perhaps a slightly increasing trend, which is consistent with the strong single-central-maximum crystal fabrics (Fig. 2c–e). There is a substantial reduction in enhancement commencing below the depth of the maximum shear strain rate. This corresponds to the region where the fabrics compatible with simple shear (i.e. a single-maximum pattern) appear to become distorted, as signified by an increase in the fabric parameter $\phi(1/4)$ discussed above. This may reflect the influence of a more complicated pattern of stresses, associated with longitudinal stresses in the portion of the ice sheet near the bedrock, associated with high relief in the surrounding regional bedrock topography.

The variable $\phi(1/4)$ does not differentiate strongly between the small circle girdle and single-central-maximum crystal fabrics, which are regarded as compatible fabrics for compression and shear, respectively. Accordingly, as an indication of the fabric development towards a girdle (or single-maximum) pattern, the ratios R_{20-30} and R_{0-15} describing the relative concentrations of c axes in the co-latitude bands 20–30° and 0–15°, have been calculated (personal communication from Li Jun, 1999). They were calculated as averages over 50 m sections and are shown in Figure 2e. If the fabric develops towards a girdle (or single maximum), the value of R_{20-30} (or R_{0-15}) will increase along with the fabric development. Based on this analysis of crystal-orientation fabrics, the evolution of crystal c-axis orientations in the DSS core has been divided into four zones (I–IV) as indicated in Figure 2e. The figure shows that the ice deformation produces crystal fabrics that become dominated by compression in the upper part of the borehole. In the first 200 m (zone I) both R_{20-30} and R_{0-15} increase

https://doi.org/10.3189/172756402781816924 Published online by Cambridge University Press

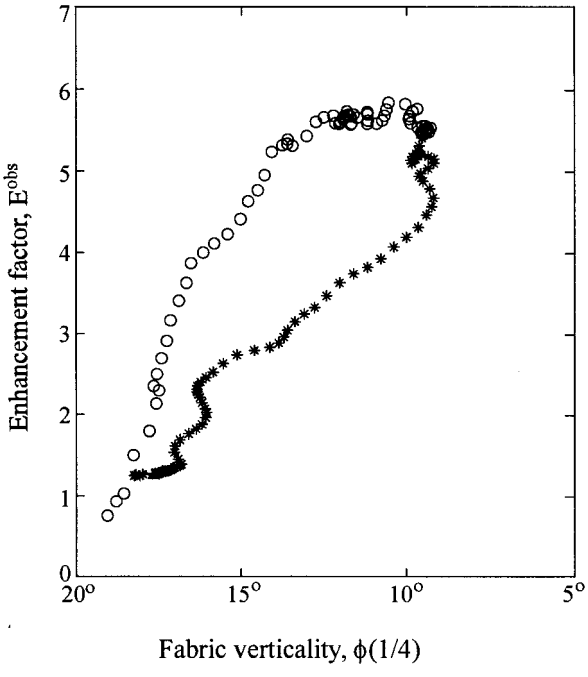

Fig. 3. The smoothed fit to the enhancement factor (E^{obs}) plotted as a function of the smoothed fabric parameter ($\phi(1/4)$). Points lying above the depth of the maximum shear strain rate are denoted (○) and those from below the maximum shear strain rate are denoted (∗). To avoid problems with smoothing, the data within the narrow spike of higher shear strain rates (see Fig. 1b), associated with the ice of the LGM, centred at 1113 m depth are not shown.

above the isotropic value, due to the disappearance of crystals with *c* axes near the horizontal plane from the initially isotropic fabrics, although the effect on R_{0-15} is small compared to the values attained for single maxima deeper in the core. In the second region, R_{0-15} generally decreases while R_{20-30} increases until 450 m depth. This zone could accordingly be interpreted as tending to group *c* axes around the girdle pattern more than about a central maximum. In zone III, R_{20-30} holds its value until about 600 m and generally takes lower values below that depth. There is a renewed increase in R_{0-15} at around 450 m which suggests that shear starts to become significant there, and there is a larger increase in R_{0-15} around 650 m, associated with a proportionate decrease in R_{20-30}, indicating the transition to the fabrics compatible with a shear-dominated stress situation. This is consistent with the appearance of the fabrics at 511 and 666 m shown in Figure 1e. The shear compatible fabrics come to dominate and this continues until around 1000 m. Below this point, in zone IV, the fabrics compatible with simple shear (i.e. single-maximum pattern) begin to become distorted as previously mentioned, and R_{0-15} is somewhat decreased. This is also reflected in a corresponding increase in $\phi(1/4)$ (Fig. 2c) in this portion of the core (except within the spike in shear strain rate associated with the LGM) back to values typical of the region around 600 m depth. This indicates an opening of the crystal fabric, suggesting that the shear stress is no longer completely dominant, and that, as previously discussed, other (presumably longitudinal and transverse) stresses, associated with proximity to the bedrock and surrounding high points in bedrock topography, are coming into play.

Finally near the bedrock (well below the LGM), multi-maxima crystal fabrics are seen, such as the one from 1153.9 m displayed in Figure 1e. These are associated with larger crystal sizes, indicative of extensive recrystallization and possible stress relaxation.

A smoothed fit to the observed enhancement factor, E^{obs} (dashed line in Fig. 2b) is plotted in Figure 3 as a function of the (smoothed) measured fabric verticality represented by $\phi(1/4)$. The figure shows that the enhancement factor increases with the strengthening of fabric verticality, but also indicates that for the same fabric verticality, the enhancement factor below the maximum shear layer value is considerably lower than that from above the maximum value. Given that these crystal fabrics are equally central (by this measure), and compatible with shear stress, one would expect proportionately similar responses to applied shear stress. This suggests that

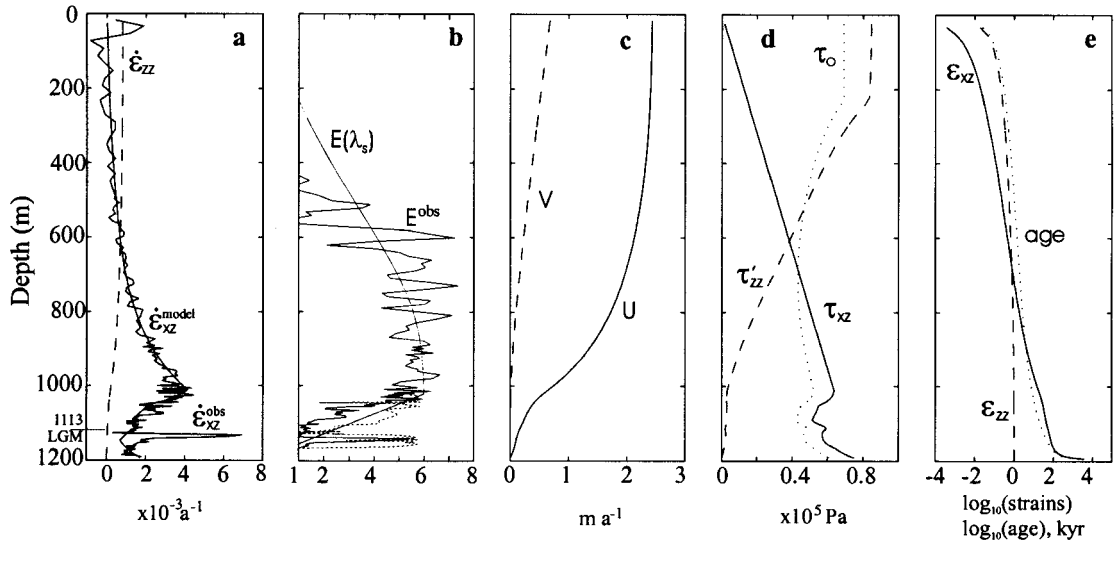

Fig. 4. Results from the model. Profiles of (a) shear strain rates ($\dot{\varepsilon}_{xz}$) from observation (thin line) and from the model (smooth line), and vertical compressive strain rate ($\dot{\varepsilon}_{zz}$) (dashed line); (b) enhancement factors E^{obs} and $E(\lambda_S)$ (solid lines), and the modified E^{obs} in the basal zone (dashed line); (c) horizontal velocity (U) and vertical velocity (V_x); (d) modified shear stress (τ_{xz}), compression stress deviator (τ'_z) and octahedral shear stress (τ_o); (e) modelled shear strain (ε_{xz}), compressive strain (ε_{zz}) and the age (dotted line) in 10^3 years.

https://doi.org/10.3189/172756402781816924 Published online by Cambridge University Press

the linear increase of shear stress with depth, which was assumed in the calculation of E^{obs}, overestimates the shear stresses below the depth of the maximum shear strain rate. Note that if we assume that other horizontal transverse and longitudinal stresses are starting to modify the fabrics below 1000 m, then there should also be additional contributions to the octahedral stress τ_{o} which would suggest that an even larger decrease in horizontal shear stress would be required. It is worth emphasizing that there is no physical requirement that the maximum shear stress τ_{xz} must occur at the base of the ice sheet. This is demonstrated by finite-element calculations of the stress fields in flowline models, such as the work of Budd and Rowden-Rich (1985) discussed in the review by Budd and Jacka (1989). The necessity to improve this aspect of application of the standard shallow-ice approximation regarding the linear depth dependence of the driving shear stress was also previously mentioned by Wang and Warner (1999).

3. MODELLING OF THE ICE DEFORMATION

The model

The previous discussion suggests that the relationship between enhancement and fabric verticality seen in Figure 3 should be regarded as more reliable above the maximum shear layer. Accordingly, the enhancement factors in the lower part of the borehole (below the maximum enhancement) were re-evaluated, based on the relation between E^{obs} and $\phi(1/4)$ above the maximum enhancement (indicated in Figure 3 by the circle symbols), using the $\phi(1/4)$ data from Figure 2c. These new enhancement factors are plotted as a dashed line in Figure 4b. This procedure assumes that the fabric verticality remains a suitable guide to enhancement for horizontal shear, and that the variation of the shear stress with depth near the bed is the uncertain quantity. For the present study we assume that the major discrepancy comes from the simple estimate of the shear stress. There would generally also be some contribution made by longitudinal stresses to the octahedral stress which would suggest that an even greater reduction in the imputed shear stress would be required, but this would be taking us out of the assumed stress configurations behind Equation (6) in any case.

New "corrected" or inferred shear stresses below the depth of maximum enhancement were accordingly determined by inserting the enhancements (E^{obs}) (obtained from the matching of enhancement and fabric verticality across the maximum shear layer as discussed above) and the observed shear strain rates (Fig. 1b) into Equation (6), leading to a marked shear stress reduction between the depth of the maximum shear strain rate and the depth of the LGM (solid line in Fig. 4d). This gives an indication of the magnitude of local stress variations that may be relevant close to the bedrock.

Observations of the vertical profiles of crystal-fabric properties are not generally available throughout ice sheets, and modelling of the evolution of such profiles in polar ice sheets is still in its infancy. Accordingly, we have used these modified shear stresses, together with a model enhancement function drawn from the analysis of laboratory ice-deformation experiments involving combined compression and shear stresses (Li and others, 1996; Warner and others, 1999; W. F. Budd and others, unpublished information) to model the expected shear strain-rate profile for DSS. This type of enhancement model (Wang and Warner, 1999) ignores the delays involved in the development of compatible crystal fabrics under changing stresses (the strain history), and relates enhancement to the nature of the applied stresses. Here we consider the simple relationship for shear flow enhancement

$$E_{xz}(\lambda_{\mathrm{S}}) = E_{\mathrm{S}}\lambda_{\mathrm{S}}\,, \tag{9}$$

where the constant E_{S} represents the enhancement appropriate to a dominant shear stress, and the shear fraction (λ_{S}) (Li and others, 1996), which ranges between 0 for dominant compression and 1 for dominant shear, may be calculated (for the geometry associated with Equations (1) and (2)) as a function of the compressive ($\dot{\varepsilon}_{zz}$) and shear strain rates ($\dot{\varepsilon}_{xz}$):

$$\lambda_{\mathrm{S}} = \frac{\dot{\varepsilon}_{xz}}{\sqrt{\dot{\varepsilon}_{xz}^2 + \dot{\varepsilon}_{zz}^2}}\,. \tag{10}$$

The value of E_{S} was taken as 6 from consideration of a large number of laboratory experiments on ice with strong single-maximum fabrics, covering a range of different stresses and temperatures, which gave enhancements ranging from 4.5 to 12. The shear flow enhancement-factor Equation (9) is based on analyses of laboratory combined stress experiments, and while it represents well the marked modification of the isotropic Glen law it is not clear how far into the compression-dominated zone it should be extrapolated. Furthermore, for the present application to Equation (6) we need to remember that our enhancement E in Equation (5) represents the enhancement of the octahedral stress–strain-rate relationship and should approach a factor describing the compressive component of deformation as λ_{S} goes to zero. As our main focus here is the shear strain-rate profile, for the present modelling study we have simply taken

$$E(\lambda_{\mathrm{S}}) = \begin{cases} E_{xz}(\lambda_{\mathrm{S}}), & \text{for} \quad E_{xz}(\lambda_{\mathrm{S}}) > 1 \\ 1, & \text{for} \quad E_{xz}(\lambda_{\mathrm{S}}) \leq 1 \end{cases} \tag{11}$$

to set the enhancement factor E to unity in the uppermost part of the ice sheet. This also gives reasonable values for E in the zone where enhanced compressive flow is expected. Using the "corrected" shear stress, this prescription of enhancement works well in the present case, except that from about 45 m below the maximum shear layer the reduction in strain rate (due to the reduced shear stress) halts and the model begins to predict progressively larger strain rates than are observed (except in the LGM spike which clearly involves other influences on flow rate), leading to a prediction close to the bedrock of nearly 10 times the observed value. Previously Wang and Warner (1999) used a model of this general type successfully in the zone above the maximum shear layer. Here we see more clearly that the formulation of shear enhancement based on Equations (9) and (10) becomes inapplicable in these lower regions. Using these equations with the observed shear and inferred vertical compression strain rates gives a shear fraction (λ_{S}) close to unity (and consequently maximal enhancement) throughout the lowest 250 m of the borehole. As discussed above, the observed enhancements and corresponding crystallographic information indicate that this is inappropriate, and laboratory experiments on large-crystal, multi-maximum basal ice also suggest that a shear enhancement factor near unity is appropriate near to the bedrock.

Accordingly, for the present study the model enhancement function is further modified, to reduce linearly to unity between the depth of maximum shear strain rate and a location about 50 m above the bottom of the borehole. This is intended to approximate the reduction of shear enhance-

https://doi.org/10.3189/172756402781816924 Published online by Cambridge University Press

ment implied by the more open crystal fabrics (larger values of $\phi(1/4)$) and the multi-maximum crystal fabrics seen within 50 m of the bedrock.

Given an initial estimate of vertical strain rate of a/D based on the observed accumulation and the total ice thickness, Equation (6) (combined with Equation (5), and the model enhancement factor described above involving Equations (8–11)) is iterated until the shear strain-rate profile, and hence the profiles of horizontal velocity, $\psi(z)$, vertical strain rate, λ_S and $E(\lambda_S)$ converge.

Results from the model

The results from the model are summarized in Figure 4. The enhanced shear strain rates ($\dot{\varepsilon}_{xz}$) are shown in Figure 4a by the smooth solid line, and the calculated enhancement, $E(\lambda_S)$, is shown in Figure 4b by a smooth line.

The shear strain-rate profile computed from the model using laboratory-determined rheology shows a good agreement with the observations from the borehole. The reduction of the shear strain rates near the bed is controlled by the counteracting combination of increased temperature, reduced shear stress and the imposed reduction in shear flow enhancement.

The base temperature at DSS is −6.9°C, which indicates that no significant basal sliding can be expected over the bedrock, so the integration of the shear strain rate over the ice column yields the horizontal velocity at the surface. The computed surface velocity (Fig. 4c) of 2.4 m a^{-1} is consistent with the value of 2.4 m a^{-1} obtained from the integration of the measured shear strain rate (Fig. 1b) over the borehole depth.

The ratio of the depth-averaged velocity to the surface velocity is calculated from the model to be 0.73, which is close to the value of 0.74 determined from the borehole velocity measurements by Morgan and others (1998), and their value of 0.76 calculated by assuming the local ice sheet is in mass balance (based on data from long-term surface elevation observations) and matching the surface accumulation rate (averaged over the last ~50 years) with the outflow around DSS determined by surface strain-rate data. The ratio of the depth-averaged velocity to the surface velocity represents the relationship between the column-integrated ice flux and measurements of the ice-sheet thickness and surface velocity. To determine the state of ice-sheet balance from the ice accumulation distributions and ice-sheet surface topography, this relationship must be considered (Budd and Warner, 1996; Wang and Warner, 1998). In areas where ice sliding can be neglected, this ratio strongly reflects the rheological properties of the ice and depends on the shear strain-rate profile through the ice column, which is influenced by the profiles of stress, temperature and ice crystal fabrics (Wang and Warner, 1998) and may be strongly affected by the large-scale bedrock roughness. Comparing these values with the value of 0.8 for a cubic flow law with isothermal isotropic ice (see Paterson, 1994, p. 251–252), at DSS the value of 0.73 is significantly smaller. This probably involves the reduced shear stresses near the bed and the distortion of the fabrics, and is also complicated by the added questions of flow within a few ice thicknesses of the Dome Summit as well as the influence of quite rough bedrock topography upstream of the drilling site (see Morgan and others, 1997, fig. 2).

The compressive and shear strains, and ice age are also calculated in the model and are shown in Figure 4e. Due to the low velocities and strain rates in the basal layers, the ice at the bottom of the DSS borehole has been computed to have undergone large strains (about 10^5% shear strain) and to be approaching 10^6 years old. This model, however, assumes steady state, and for such long times the non-steady-state variations associated with the ice-age cycles would need to be taken into account.

4. SUMMARY AND CONCLUSIONS

The ice-flow properties at the DSS borehole have been studied in this paper from a combination of data including the analysis of the ice cores and observed shear rates measured in the borehole. Consideration of the temperature-dependent nature of ice flow, the cubic non-linear nature of the ice-flow relations, and the standard Glen-type flow dependence on the octahedral stress does not explain the observed variation of shear strain rate measured in the borehole, and it was possible to infer the nature of the required enhancement factor, associated primarily with the shear flow. This enhancement showed a strong correlation with ice crystal-fabric verticality, which was used to infer how the shear stress might deviate in the region of the borehole below the high shear layer. This correlation could also provide a starting point for a direct description of enhanced flow relations as a function of the state of the crystal fabric. It would be of interest to compare our results with an explicit fabric-based model of anisotropic ice flow such as that of Azuma and Goto-Azuma (1996). The observed relationship between enhancement and fabric could also be combined (to provide the flow dynamics) with models that describe the evolution of fabrics within a flowing ice sheet.

The shear strain-rate profile, calculated from a model description of enhancement based on laboratory ice-deformation experiments for anisotropic ice under combined compression and shear, also provided reasonable agreement with the observations above the maximum shear layer. That model relies on the fact that once the shear strain rate becomes comparable with compressive strain rate, it rapidly dominates it, and soon imparts a sufficient cumulative shear strain to enable the ice to develop a crystal-orientation fabric compatible with the stress configuration. The model involves parameterizing the enhancement (with a primary focus on the shear flow rate) in terms of the stress parameter λ_S, and thus avoids requiring detailed information about the ice crystal fabric. In the present example, a very simple relation between the shear fraction and the enhancement gave useful results above the high shear layer.

In general, as we have seen in previous studies (Wang and Warner, 1998, 1999; Wang 2000), the inclusion of specific ice-flow relations, linked to experimental measurements of ice flow, makes it clear that a more detailed treatment is needed to describe the flow in the lowest sections of an ice sheet. In the present application to the Law Dome DSS borehole it was possible to argue for separate reduced enhancements and reduced shear stresses below the high shear layer, by combining the picture of anisotropic flow enhancement with information about the crystal fabrics.

REFERENCES

Azuma, N. and K. Goto-Azuma. 1996. An anisotropic flow law for ice-sheet ice and its implications. *Ann. Glaciol.*, **23**, 202–208.

Budd, W. F. and T. H. Jacka. 1989. A review of ice rheology for ice sheet

https://doi.org/10.3189/172756402781816924 Published online by Cambridge University Press

modelling. *Cold Reg. Sci. Technol.*, **16**(2), 107–144.
Budd, W. F. and R. J. M. Rowden-Rich. 1985. Finite element analysis of two-dimensional longitudinal section flow on Law Dome. *AANARE Res. Notes* 28, 153–161.
Budd, W. F. and R. C. Warner. 1996. A computer scheme for rapid calculations of balance-flux distributions. *Ann. Glaciol.*, **23**, 21–27.
Curran, M. A. J., T. D. van Ommen and V. Morgan. 1998. Seasonal characteristics of the major ions in the high-accumulation Dome Summit South ice core, Law Dome, Antarctica. *Ann. Glaciol.*, **27**, 385–390.
Dahl-Jensen, D. 1985. Determination of the flow properties at Dye 3, south Greenland, by bore-hole-tilting measurements and perturbation modelling. *J. Glaciol.*, **31**(108), 92–98.
Dahl-Jensen, D. and N. S. Gundestrup. 1987. Constitutive properties of ice at Dye 3, Greenland. *International Association of Hydrological Sciences Publication* 170 (Symposium at Vancouver 1987 — *The Physical Basis of Ice Sheet Modelling*), 31–43.
Edwards, R., P. N. Sedwick, V. Morgan, C. F. Boutron and S. Hong. 1998. Iron in ice cores from Law Dome, East Antarctica: implications for past deposition of aerosol iron. *Ann. Glaciol.*, **27**, 365–370.
Etheridge, D. M. 1989. Dynamics of the Law Dome ice cap, Antarctica, as found from bore-hole measurements. *Ann. Glaciol.*, **12**, 46–50.
Glen, J. W. 1955. The creep of polycrystalline ice. *Proc. R. Soc. London, Ser. A*, **228**(1175), 519–538.
Glen, J. W. 1958. The flow law of ice: a discussion of the assumptions made in glacier theory, their experimental foundation and consequences. *International Association of Scientific Hydrology Publication* 47 (Symposium at Chamonix 1958 — *Physics of the Movement of the Ice*), 171–183.
Li Jun. 1995. Interrelation between flow properties and crystal structure of snow and ice. (Ph.D. thesis, University of Melbourne.)
Li Jun, T. H. Jacka and W. F. Budd. 1996. Deformation rates in combined compression and shear for ice which is initially isotropic and after the development of strong anisotropy. *Ann. Glaciol.*, **23**, 247–252.
Li Jun, T. H. Jacka and V. Morgan. 1998. Crystal-size and microparticle record in the ice core from Dome Summit South, Law Dome, East Antarctica. *Ann. Glaciol.*, **27**, 343–348.
Morgan, V. I., C. W. Wookey, Li Jun, T. D. van Ommen, W. Skinner and M. F. Fitzpatrick. 1997. Site information and initial results from deep ice drilling on Law Dome, Antarctica. *J. Glaciol.*, **43**(143), 3–10.
Morgan, V., T. D. van Ommen, A. Elcheikh and Li Jun. 1998. Variations in shear deformation rate with depth at Dome Summit South, Law Dome, East Antarctica. *Ann. Glaciol.*, **27**, 135–139.
Paterson, W. S. B. 1994. *The physics of glaciers. Third edition*. Oxford, etc., Elsevier.
Rosman, K. J. R. *and 6 others*. 1998. Lead isotopes and selected metals in ice from Law Dome, Antarctica. *Ann. Glaciol.*, **27**, 349–354.
Russell-Head, D. S. and W. F. Budd. 1979. Ice-sheet flow properties derived from bore-hole shear measurements combined with ice-core studies. *J. Glaciol.*, **24**(90), 117–130.
Thorsteinsson, T., E. D. Waddington, K. C. Taylor, R. B. Alley and D. D. Blankenship. 1999. Strain-rate enhancement at Dye 3, Greenland. *J. Glaciol.*, **45**(150), 338–345.
Wang, W. L. 1994. Laboratory studies of flow properties and associated crystal structure in Holocene and Wisconsin ice. (M.Sc. thesis, University of Tasmania.)
Wang, W. L. 2000. Incorporation of rheological properties into ice sheet flow models. (Ph.D. thesis, University of Tasmania.)
Wang, W. L. and R. C. Warner. 1998. Simulation of the influence of ice rheology on velocity profiles and ice-sheet mass balance. *Ann. Glaciol.*, **27**, 194–200.
Wang, W. L. and R. C. Warner. 1999. Modeling of anisotropic ice flow in Law Dome, East Antarctica. *Ann. Glaciol.*, **29**, 184–190.
Warner, R. C., T. H. Jacka, J. Li and W. F. Budd. 1999. Tertiary flow relations for compression and shear components in combined stress tests on ice. *In* Hutter, K., Y. Wang and H. Beer, *eds. Advances in cold-region thermal engineering and sciences: technological, environmental, and climatological impact*. Berlin, etc., Springer-Verlag, 259–270. (Lecture Notes in Physics 533.)
Weertman, J. 1973. Creep of ice. *In* Whalley, E., S. J. Jones and L. Gold, eds. *Physics and chemistry of ice*. Ottawa, Ont., Royal Society of Canada, 320–337.

https://doi.org/10.3189/172756402781816924 Published online by Cambridge University Press